Statistical wave field theory: Special polyhedra

Roland Badeau[a]

[a]*LTCI, Télécom Paris, Institut Polytechnique de Paris, Palaiseau, 91120, France*

Abstract

The statistical wave field theory establishes mathematically the statistical laws of the solutions to the wave equation in a bounded volume. It provides the closed-form expression of the power distribution and the correlations of the wave field jointly over time, frequency and space, in terms of the geometry and the specific admittance of the boundary surface. In a recent paper, we presented a mathematical approach to this theory based on the Sturm-Liouville theory and the theory of dynamical billiards. We focused on mixing billiards that generate an isotropic wave field, and we retrieved the well-known statistical properties of reverberation in room acoustics. In the present paper, we introduce a simpler geometric approach, dedicated to a particular class of non-ergodic billiards. Though limited to only a few polyhedra, this approach offers a precious insight into various aspects of the theory, including the first examples of anisotropic wave fields, whose statistical properties are related to mathematical crystallography. We also show that the formulas that we obtain in this anisotropic case are closely related to those of the mixing case, albeit based on a different mathematical approach.

Keywords: Statistical physics, wave equation, Helmholtz equation, reverberation

Contents

Email address: roland.badeau@telecom-paris.fr (Roland Badeau)

1. Introduction

In the field of room acoustics, it is well known that when waves propagate in a bounded three-dimensional space, after many reflections on the room boundaries, and at high frequency, their collective behavior becomes stochastic, a physical phenomenon that is called *late reverberation*. During the 20th century, several researchers aimed to characterize mathematically various statistical properties of reverberation, *e.g.* over time (Moorer, 1979), frequency (Schroeder, 1962), time-frequency (Polack, 1988) and space (Cook *et al.*, 1955). In particular, the reverberation time, which is defined as the time it takes for the sound pressure level to reduce by 60 dB, received special attention, first with the empirical law proposed by Sabine at the end of the 19th century from early experiments, which holds in a diffuse acoustic field and highly reverberant rooms (Joyce, 1975), then with the modified formula established by Eyring (1930), which holds when the absorption at the boundary is larger, and later with the reverberation theory of Polack (1992), based on the mathematical theory of dynamical billiards (Tabachnikov, 1995).

Indeed, at high frequency, wave propagation can be approximated by considering the trajectory of rays that undergo successive specular reflections on the domain's boundary, similarly to optical rays (Kuttruff, 2014, Chap. 4). The ray trajectory can then be interpreted as a dynamical billiard that, depending on the boundary geometry, may follow different statistical properties. For instance, a billiard is *ergodic* when over time, the position and the unit direction vector of almost every ray trajectory are jointly uniformly distributed in the *phase space* $V \times \mathcal{S}(0,1)$, where V denotes the bounded volume and $\mathcal{S}(0,1)$ is the unit sphere. In addition, *mixing* billiards, in addition to being ergodic, are such that after an asymptotically long elapsed time, the orientation of the ray at any receiver's position is

statistically independent of the source's position and orientation. Under this assumption, the wave field statistics are independent of the receiver's position and orientation in the room. The wave field is thus isotropic (so the classical definition of a *diffuse field* can be considered as equivalent to the mixing property), and the reverberation time is also independent of the space position and the orientation in the room (Polack, 1992). In other respects, even in rooms whose shape is not mixing, Joyce (1978) proved that replacing the deterministic specular reflections with random reflections following Lambert's cosine law was sufficient to enforce ergodicity. In ergodic rooms, various formulas have been proposed for the asymptotic reverberation time, based on the statistics of the reflections on the boundary surface, see *e.g.* Joyce (1978), Polack (1992) and Kuttruff (2014, Chaps. 4 and 5). Yet, the case of non-ergodic rooms is much more complex, since the reverberation time can no longer be uniquely defined, and may depend on the source and receiver positions and orientations. A noteworthy study of the particular case of bidimensional (2D) and three-dimensional (3D) ergodic and non-ergodic circular and rectangular enclosures can be found in Polack (2024).

In a recent publication (Badeau, 2024), the author of the present paper has opted for a radically different mathematical approach, which proved to be much more powerful than the usual methods based on the statistics of the reflections. This innovative approach led to a whole new theory called *statistical wave field theory*. This theory establishes mathematically the statistical laws of the solutions to the wave equation in a bounded volume. It provides the closed-form expression of the power distribution and the correlations of the wave field jointly over time, frequency and space, in terms of the geometry and the specific admittance of the boundary surface. In room acoustics, it permitted us to retrieve the well-known statistical properties of reverberation that have been established over the past century, and to reveal new, previously unknown properties.

In Badeau (2024), we focused on the case of mixing rooms, and we developed a complex mathematical approach based on a Weyl-like asymptotic expansion of the modal density (Balian and Bloch, 1970). So, one of the objectives of the present paper is to introduce a simpler and more intuitive geometric approach to the statistical wave field theory. For this purpose, we address a simpler framework than that of mixing billiards: we consider polyhedral shapes V, which will be referred to as *special polyhedra* and which include the rectangular cuboid as a particular case, that are neither mixing nor ergodic, but rather *integrable* in the sense of Arnold's theorem (Arnold and Avez, 1989). This means that the Helmholtz equation can be solved in closed-form subject to various boundary conditions (Dirichlet, Neumann, and even Robin in certain cases). Moreover, all the eigenfunctions are trigonometric polynomials. Based on these closed-form solutions, deriving the equations of the statistical wave field theory will prove to be much easier than in the mixing case. Moreover, a notable difference with the mixing case is that the high frequency approximation is not even required: the theory predictions hold right from the zero frequency.

In the case of Neumann's boundary condition, we will then show that the wave field in these special polyhedra is stationary but not isotropic. Yet, its second order statistics present the rotational invariances of a cyclic crystallographic point group. In the case of Robin's boundary condition, we will show that the wave vector space undergoes a nonlinear

distortion and that this distortion is not isotropic either, but presents the same rotational invariances of a cyclic crystallographic point group. This new approach paves the way for a general anisotropic formula of the reverberation time, which encompasses both cases of special polyhedra and mixing billiards.

This paper is structured accordingly to Badeau (2024), in order to permit an easy comparison of the two documents. Note that Badeau (2024) includes a comprehensive literature review, as well as detailed information regarding the various assumptions, concepts and implications of the statistical wave field theory, which will not be repeated here, in order to avoid unneeded redundancies. Nevertheless, the present paper is written so that it can be read independently from Badeau (2024). Sec. 2 introduces some acronyms and mathematical notations that will be used in the rest of the paper. Then Sec. 3 characterizes the sets of polyhedra that are the subject of the present study, and Sec. 4 summarizes a few fundamental notions regarding wave propagation that are needed to develop the theory. Section 5 reviews the mathematical assumptions on which the theory relies in the particular case of special polyhedra. Then Sec. 6 develops the *special* theory dedicated to Neumann's boundary condition, and Sec. 7 develops the *general* theory dedicated to Robin's boundary condition. Section 8 compares the results obtained in the case of special polyhedra with those already obtained in the case of mixing billiards (Badeau, 2024). Finally, Sec. 9 summarizes the main contributions of this paper, and proposes a few perspectives for future work.

2. Acronyms and mathematical notations

Acronyms:

ACF auto-covariance function

WSS wide sense stationary

Mathematical notations:

- $\triangleq$: equal by definition to
- $\mathbb{N}$: set of whole numbers
- $\mathbb{R}$, $\mathbb{C}$: sets of real and complex numbers
- $\imath = \sqrt{-1}$: imaginary unit
- $\mathbb{R}_+$: set of nonnegative real numbers
- $\boldsymbol{x}$ (bold font), z (regular): vector and scalar, respectively
- $A \backslash B$: relative complement (set difference) of set B in set A
- $A^* = A \backslash \{0\}$: set A minus 0
- $A \subseteq B$: A is a subset of B, possibly equal to B

- $\mathring{V}$: interior of a subset V of $\mathbb{R}^3$
- $\overline{V}$: closure of a subset V of $\mathbb{R}^3$
- $|V|$: Lebesgue measure (volume) of a subset V of $\mathbb{R}^3$
- $\lambda = \frac{1}{|V|}$: mean density of sources over space
- $\partial V = \overline{V} \backslash \mathring{V}$: boundary of a subset V of $\mathbb{R}^3$
- $\boldsymbol{n}(\boldsymbol{x})$ where $\boldsymbol{x} \in \partial V$: outward unit normal vector to the boundary surface of subset V
- $S(A)$: area of a 2D sub-manifold A of $\mathbb{R}^3$
- $\boldsymbol{P}_S$: 3×2 orthonormal matrix whose range space is parallel to the flat surface S
- $\|.\|_2$: Euclidean/Hermitian norm of a vector or a function
- $\overline{z}$: complex conjugate of $z \in \mathbb{C}$
- $\mathrm{Re}(z)$ (resp. $\mathrm{Im}(z)$): real (resp. imaginary) part of a complex number $z \in \mathbb{C}$
- $\boldsymbol{x}^\top$: transpose of vector $\boldsymbol{x}$
- $A^\perp$: orthogonal complement of set A
- $\mathcal{S}(\mathbf{0}, k)$: sphere centered at the origin and of radius k: $\mathcal{S}(\mathbf{0}, k) = \{\boldsymbol{k} \in \mathbb{R}^3; \|\boldsymbol{k}\|_2 = k\}$
- C_n: finite group of rotations that is generated by a unique rotation of angle $\frac{2\pi}{n}$
- SO(3): special orthogonal group (3D rotation group)
- $L^2(V)$ where V is a Borel subset of $\mathbb{R}^3$: Hilbert space of measurable functions f supported in V, such that $\|f\|_2 = \sqrt{\int_V |f(\boldsymbol{x})|^2 d\boldsymbol{x}} < +\infty$
- δ_{n_1,n_2}: Kronecker delta: $\delta_{n_1,n_2} = 1$ if $n_1 = n_2$, $\delta_{n_1,n_2} = 0$ otherwise
- $\delta(.)$: Dirac delta function
- $\mathrm{Ш}_L$ with $L > 0$: Dirac comb defined on $\mathbb{R}$: $\mathrm{Ш}_L(x) = \sum_{k \in \mathbb{Z}} \delta(x - kL)$
- $\Delta\phi(\boldsymbol{x})$: Laplacian of function $\phi(\boldsymbol{x})$
- 1D Fourier transform of function $\psi : \mathbb{R} \to \mathbb{C}$:

$$\widehat{\psi}(\nu) = \int_{t \in \mathbb{R}} \psi(t) e^{-2\imath\pi\nu t} dt \tag{1}$$

- 3D Fourier transform of function $\psi : \mathbb{R}^3 \to \mathbb{C}$:

$$\widehat{\psi}(\boldsymbol{k}) = \int_{\boldsymbol{x} \in \mathbb{R}^3} \psi(\boldsymbol{x}) e^{-2\imath\pi\boldsymbol{k}^\top \boldsymbol{x}} d\boldsymbol{x} \tag{2}$$

- $\mathbb{E}[X]$: expected value of a random variable X
- Covariance of two complex random variables X and Y:

$$\operatorname{cov}[X, Y] = \mathbb{E}[(X - \mathbb{E}[X])\overline{(Y - \mathbb{E}[Y])}]$$

3. Special polygons and polyhedra

In this section, we characterize the sets of special polygons and special polyhedra that are integrable in the sense of Arnold's theorem (Arnold and Avez, 1989), which means that the Helmholtz equation can be solved in closed-form subject to various boundary conditions (Dirichlet, Neumann, and even Robin in certain cases).

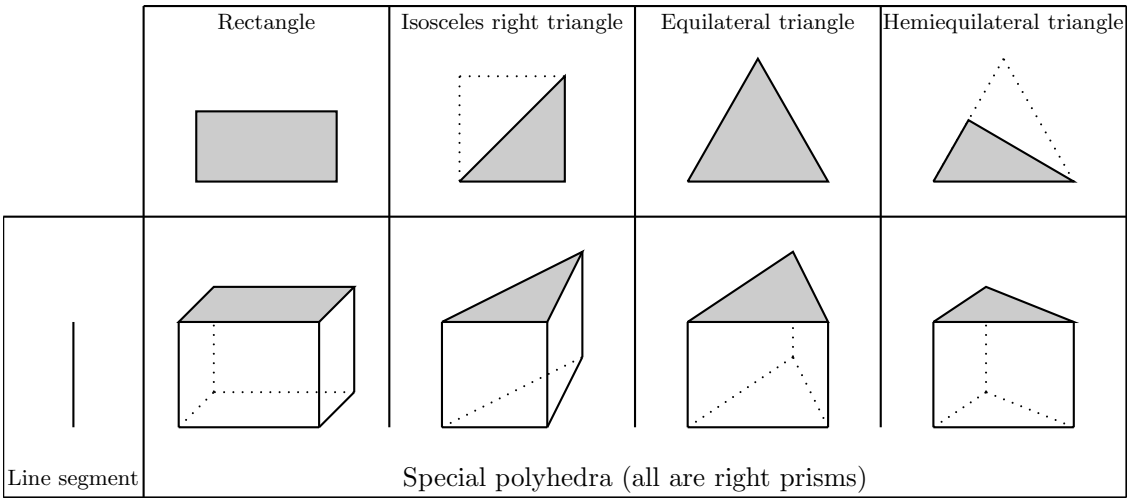

Figure 1: Special polygons and the corresponding special polyhedra

First, in two space dimensions, there exist only four integrable polygons (Amar *et al.*, 1991; McCartin, 2008), which are illustrated in Fig. 1, and which will be referred to as *special polygons*. Indeed, it is necessary that every angle between two sides be equal to $\frac{\pi}{n}$ for some $n \in \mathbb{N}^*$, so that the number of sides can only be 3 or 4, the only possible quadrilateral being the rectangle. In the case of triangles, the three angles have to sum to π, so the only possible values of n are 2, 3, 4 and 6. This suggests a relationship with the crystallographic restriction theorem (Bamberg *et al.*, 2003), as proved in Rowlett *et al.* (2021). More precisely, only three triangles are admissible: the isosceles right triangle (whose angles are $\frac{\pi}{2}, \frac{\pi}{4}, \frac{\pi}{4}$), the equilateral triangle (whose angles are $\frac{\pi}{3}, \frac{\pi}{3}, \frac{\pi}{3}$), and the hemiequilateral triangle (whose angles are $\frac{\pi}{2}, \frac{\pi}{3}, \frac{\pi}{6}$). Among these special polygons, the eigenfunctions of the rectangle can be easily expressed in Cartesian coordinates as the outer product of two one-dimensional (1D) eigenfunctions of the line segment, the eigenfunctions of the equilateral triangle were originally solved in closed-form by Lamé (1833), and the eigenfunctions of the isosceles right triangle and the hemiequilateral triangle are deduced from those of the square and

the equilateral triangle, respectively [see McCartin (2011) for a study of the equilateral and hemiequilateral triangles, and Overfelt and White (1986) for a study of the isosceles right triangle].

In higher space dimension n, the characterization of the geometric shapes that admit a complete set of trigonometric eigenfunctions is still an open problem. Rowlett *et al.* (2021) and Blom (2021) conjecture that a necessary and sufficient condition is that V is a polytope that strictly tessellates space, which means that $\mathbb{R}^n = \cup_{j\in\mathbb{Z}} V_j$, where all V_j are isometric to V, and are obtained by reflecting V across its boundary faces. Furthermore, the hyperplanes that contain the boundary faces of each V_j must have empty intersection with the interior of V_k, for all j and k.

In three space dimensions, to the best of our knowledge, there exist only four polyhedra that strictly tessellate $\mathbb{R}^3$, and that indeed admit a complete set of trigonometric eigenfunctions: all of them are right prisms, whose polygonal base is one of the four special polygons. Their eigenfunctions are thus expressed as the product of a 2D eigenfunction of their polygonal base and a 1D eigenfunction of the line segment. These four special polyhedra are illustrated in Fig. 1. It is worth noticing that in these integrable dynamical billiards, the phase space is not explored in an ergodic manner, because the ray trajectories switch over time between only a finite number of directions. Nevertheless, almost every ray trajectory still reaches almost all positions in V uniformly over time, which means that space is still explored in an ergodic manner.

4. Fundamentals of waves revisited

This section summarizes a few fundamental notions regarding wave propagation that are needed in the rest of the paper. Most of these notions are well-known and are described for instance in Morse and Ingard (1968). These and other notions were already presented in more details in Badeau (2024, Sec. III), except for the particular case of special polyhedra that is addressed in Secs. 4.3.2 and 4.4.2.

4.1. Main definitions

In a simply connected open domain $V \subseteq \mathbb{R}^3$, the homogeneous wave equation states that

$$\Delta p(\boldsymbol{x}, t) - \frac{1}{c^2}\frac{\partial^2 p(\boldsymbol{x}, t)}{\partial t^2} = 0, \tag{3}$$

where $p(\boldsymbol{x}, t)$ is the wave amplitude at position $\boldsymbol{x} \in V$ and time $t \in \mathbb{R}$, Δ is the Laplacian, and c is the propagation speed of the wave. Applying the 1D Fourier transform (Eq. (1)) with respect to time to Eq. (3) yields the Helmholtz equation:

$$\Delta\phi(\boldsymbol{x}) + 4\pi^2 k^2 \phi(\boldsymbol{x}) = 0, \tag{4}$$

where the scalar $k = \frac{\nu}{c}$ is the *wave number* and ν denotes the frequency.

Given a punctual source position $\boldsymbol{x}_0 \in V$ and a space position $\boldsymbol{x} \in V$, a Green's function G of the Helmholtz equation is a particular solution of the following inhomogeneous Helmholtz equation:

$$\Delta G(\boldsymbol{x}, \boldsymbol{x}_0, k) + 4\pi^2 k^2 G(\boldsymbol{x}, \boldsymbol{x}_0, k) = -\delta(\boldsymbol{x} - \boldsymbol{x}_0). \tag{5}$$

4.2. B-function

In the case of a simply connected domain $V \subset \mathbb{R}^3$ with boundaries, any Green's function $G(\boldsymbol{x}, \boldsymbol{x}_0, k)$ can generally be analytically continued on a mathematical vicinity $\mathcal{D}$ of V that depends on the geometry and the specific admittance of the boundary surface. In some cases, this extension holds in the full space $\mathcal{D} = \mathbb{R}^3$. The B-function on $\mathcal{D} \subseteq \mathbb{R}^3$ is then defined as:

$$B(\boldsymbol{y}, \boldsymbol{x}_0, k) = -\left(\Delta G(\boldsymbol{y}, \boldsymbol{x}_0, k) + 4\pi^2 k^2 G(\boldsymbol{y}, \boldsymbol{x}_0, k)\right). \tag{6}$$

By definition of the Green's function G in Eq. (5), the restriction of the B-function to V is $\delta(\boldsymbol{y} - \boldsymbol{x}_0)$. Reciprocally, when $\mathcal{D} = \mathbb{R}^3$, a particular Green's function G is obtained as:

$$G(\boldsymbol{x}, \boldsymbol{x}_0, k) = \int_{\boldsymbol{y} \in \mathbb{R}^3} G_0(\boldsymbol{x} - \boldsymbol{y}, k)\, B(\boldsymbol{y}, \boldsymbol{x}_0, k) d\boldsymbol{y}, \tag{7}$$

where G_0 is a free-field Green's function. Equation (7) permits us to interpret the B-function as a spatial distribution of image sources in the free field, which collectively generate inside V the same response as that of the single original source within the bounded domain V. In this paper, we will focus on Neumann's boundary condition and on the special polyhedra, in which case the B-function is real-valued, defined on $\mathcal{D} = \mathbb{R}^3$, and does not depend on k, so it will be simply denoted $B(\boldsymbol{y}, \boldsymbol{x}_0)$.

4.3. Neumann's boundary condition

Let us consider a simply connected domain $V \subsetneq \mathbb{R}^3$, whose boundary ∂V is a Lipschitz continuous 2D manifold (i.e. ∂V is locally the graph of a Lipschitz function). Then Neumann's boundary condition of the Helmholtz equation (4) states that

$$\forall \boldsymbol{x} \in \partial V,\ \frac{\partial \phi(\boldsymbol{x})}{\partial \boldsymbol{n}(\boldsymbol{x})} = 0, \tag{8}$$

where ∂V denotes the boundary surface of V, and $\frac{\partial}{\partial \boldsymbol{n}(\boldsymbol{x})}$ denotes partial differentiation in the direction of the outward normal to this surface at $\boldsymbol{x}$. In room acoustics, Eq. (8) models the reflection of sound waves by *hard* (or *rigid*) surfaces, which reflect the wave without absorbing any energy (Kuttruff, 2014, Chap. 3).

4.3.1. Simply connected bounded domain

If V is a bounded domain, then the Sturm-Liouville theory (Pearson, 2001) shows that the set of *eigenvalues* k_n and unit *eigenfunctions* $\phi_n(\boldsymbol{x})$, also called *normal modes*, which are solutions to Eqs. (4) and (8) is discrete: it is indexed by $n \in \mathbb{N}$. Moreover, both k_n and $\phi_n(\boldsymbol{x})$ are real. So, without loss of generality, the eigenvalues k_n can be assumed nonnegative and sorted by non-decreasing order. Finally, the set $\{\phi_n(\boldsymbol{x})\}_{n \in \mathbb{N}}$ is such that

$$\forall \boldsymbol{x}, \boldsymbol{y} \in V,\ \sum_{n \in \mathbb{N}} \phi_n(\boldsymbol{x}) \phi_n(\boldsymbol{y}) = \delta(\boldsymbol{x} - \boldsymbol{y}). \tag{9}$$

This set forms a Hilbert basis of the real Hilbert space $L^2(V)$ of square-integrable functions on V. In addition, note that the constant function $\phi_0(\boldsymbol{x}) = \frac{1}{\sqrt{|V|}}$ is always a unit eigenfunction of Eqs. (4)) and (8), of eigenvalue $k_0 = 0$.

Then given a punctual source position $\boldsymbol{x}_0 \in V$, let us consider the following Green's function of the Helmholtz equation (4), which satisfies Eq. (5):

$$G(\boldsymbol{x}, \boldsymbol{x}_0, k) = \sum_{n \in \mathbb{N}} \frac{\phi_n(\boldsymbol{x}_0)\, \phi_n(\boldsymbol{x})}{4\pi^2 (k_n^2 - k^2)}. \tag{10}$$

Finally, every eigenfunction $\phi_n(.)$ is holomorphic in V, so it can be continued as an analytic function on a mathematical vicinity $\mathcal{D}$ of V, which is a solution of the Helmholtz equation (4) on $\mathcal{D}$. Substituting Eqs. (4) and (10) into Eq. (6) yields the closed-form expression of the B-function on $\mathcal{D}$:

$$B(\boldsymbol{y}, \boldsymbol{x}_0) = \sum_{n \in \mathbb{N}} \phi_n(\boldsymbol{x}_0)\, \phi_n(\boldsymbol{y}). \tag{11}$$

Note that Eq. (9) confirms that the restriction of the B-function to V is $\delta(\boldsymbol{y} - \boldsymbol{x}_0)$, as already mentioned in Sec. 4.2.

4.3.2. Special polyhedra

As mentioned in Sec. 1, the special polyhedra belong to the few geometric shapes for which the eigenvalues k_n and eigenfunctions $\phi_n(\boldsymbol{x})$, which satisfy Eqs. (4) and (8), can be calculated in closed-form. For instance, in 2D, the equilateral triangle and the hemiequilateral triangle are solved in McCartin (2002), and the isosceles right triangle is solved in Overfelt and White (1986). In 3D, the corresponding right prisms represented in Fig. 1 are solved in the same way, as the outer product of each of these triangles and the line segment. From these closed-form expressions, the B-function can then be also calculated in closed-form, and it appears that it is always an atomic measure defined on $\mathcal{D} = \mathbb{R}^3$, whose support is the finite union of translates of a certain lattice, as illustrated in Fig. 2 in the 2D case.

In this section, we will first focus on the particular case of the rectangular cuboid, because it is both the simplest case to solve mathematically, and the principal case of interest in room acoustics (Kuttruff, 2014, Chap. 3). Then we will introduce a common mathematical framework that applies to all special polyhedra.

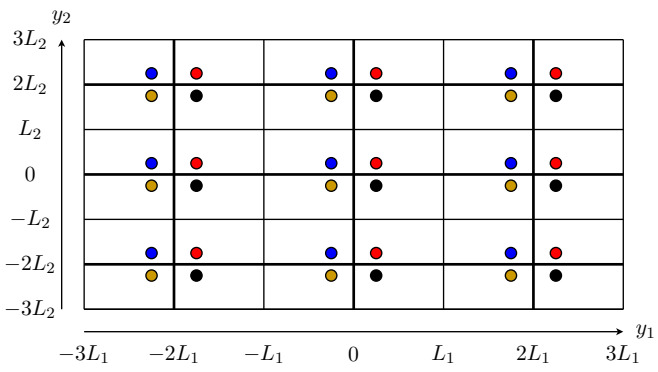

(a) Periodic space tessellation by the rectangle (primitive unit cells bordered by thick lines)

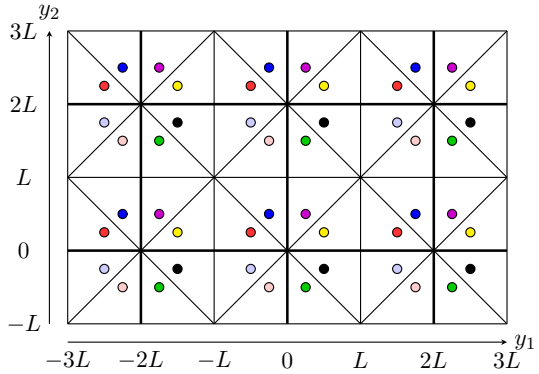

(b) Periodic space tessellation by the isosceles right triangle (primitive unit cells bordered by thick lines)

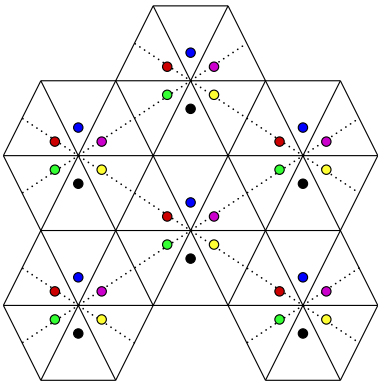

(c) Periodic space tessellation by the equilateral triangle (primitive unit cells bordered by dotted lines)

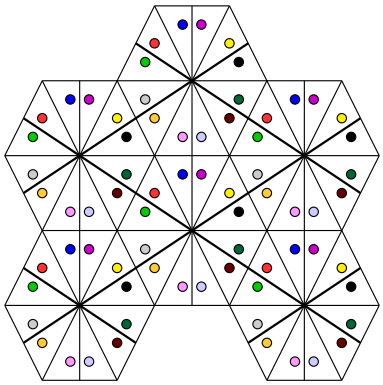

(d) Periodic space tessellation by the hemiequilateral triangle (primitive unit cells bordered by thick lines)

Figure 2: Periodic B-function (atoms represented with colors) and strict space tessellation by special polygons

Rectangular cuboid. Let us consider a rectangular cuboid of dimensions L_1, L_2, L_3, so that $V{=}(0, L_1) \times (0, L_2) \times (0, L_3)$. Then the normal modes can be indexed by three natural numbers $(n_1, n_2, n_3) \in \mathbb{N}^3$, with eigenvalues $k_{n_1,n_2,n_3} = \frac{1}{2}\sqrt{\frac{n_1^2}{L_1^2} + \frac{n_2^2}{L_2^2} + \frac{n_3^2}{L_3^2}}$, and eigenfunctions

$$\begin{aligned} \phi_{n_1,n_2,n_3}(\boldsymbol{x}) = &\ 2^{-\frac{\delta_{n_1,0}+\delta_{n_2,0}+\delta_{n_3,0}}{2}} \sqrt{\tfrac{8}{|V|}} \prod_{l=1}^{3} \cos\left(\tfrac{\pi n_l x_l}{L_l}\right) \\ = &\ \frac{2^{-\frac{\delta_{n_1,0}+\delta_{n_2,0}+\delta_{n_3,0}}{2}}}{\sqrt{8|V|}} \sum\nolimits_{s_1,s_2,s_3=\pm 1} e^{2\imath\pi \boldsymbol{k}_{s_1 n_1, s_2 n_2, s_3 n_3}^{\top} \boldsymbol{x}}, \end{aligned} \tag{12}$$

where the wave vectors are indexed by three integers $(n_1, n_2, n_3) \in \mathbb{Z}^3$:

$$\boldsymbol{k}_{n_1,n_2,n_3} = \left[\tfrac{n_1}{2L_1}, \tfrac{n_2}{2L_2}, \tfrac{n_3}{2L_3}\right]^{\top}. \tag{13}$$

Substituting Eq. (12) into Eq. (11) yields the following closed-form expression of the B-function, which is defined on $\mathcal{D} = \mathbb{R}^3$:

$$B(\boldsymbol{y}, \boldsymbol{x}_0) = \prod_{l=1}^{3} \sum_{s_l = \pm 1} \text{Ш}_{2L_l}(y_l - s_l\, x_{0l}),$$

where Ш_L denotes the Dirac comb of period $L > 0$. An example of this B-function is illustrated in Fig. 2(a) in the 2D-case, where its atoms are represented with different colors, so as to highlight its periodicity. It can be noticed that the successive reflections of the original domain $V = (0, L_1) \times (0, L_2)$ strictly tessellate the 2D space, and that the B-function is periodic of primitive unit cell $(0, 2L_1) \times (0, 2L_2)$ (which is bordered by thick lines in Fig. 2(a)), repeated on a rectangular Bravais lattice (Bravais, 1850).

General case. The B-functions of the three other special polyhedra are illustrated in Figs. 2(b)-(d) in the 2D case. It can be noticed that the B-function is always a periodic atomic measure, and that its primitive unit cell is always a parallelogram, which is bordered by thick lines in Figs. 2(a),(b),(d), and by dotted lines in Fig. 2(c), because in the particular case of the equilateral triangle, these lines do not match the edges of the domain V.

Mathematically, the eigenfunctions $\phi_n(\boldsymbol{x})$ of the four special polyhedra are trigonometric polynomials. We can thus write: $\forall n \in \mathbb{N}$,

$$\phi_n(\boldsymbol{x}) = \sum_m \alpha_{n,m} e^{2\imath\pi \boldsymbol{k}_{n,m}^\top \boldsymbol{x}} \tag{14}$$

where, without loss of generality, the finite set of parameters $\alpha_{n,m} \in \mathbb{C}$ and $\boldsymbol{k}_{n,m} \in \mathbb{R}^3$ can be indexed so as to satisfy the following properties:

- the wave vectors $\{\boldsymbol{k}_{n,m}\}_{n,m}$ are distributed on a Bravais lattice in $\mathbb{R}^3$;
- $\forall n \in \mathbb{N}$, the wave vectors $\boldsymbol{k}_{n,m}$ have the same norm: $\forall m,\ \|\boldsymbol{k}_{n,m}\|_2 = k_n$;
- $\forall n \in \mathbb{N}$, since $\phi_n(\boldsymbol{x})$ is real-valued, we have

$$\forall m,\ \boldsymbol{k}_{n,-m} = -\boldsymbol{k}_{n,m} \text{ and } \alpha_{n,-m} = \overline{\alpha}_{n,m}; \tag{15}$$

- finally, since the eigenfunctions are unitary (i.e. $\int_V \phi_n(\boldsymbol{x})^2 d\boldsymbol{x} = 1$), we have

$$\forall n \in \mathbb{N},\ \sum_m |\alpha_{n,m}|^2 = \lambda \triangleq \tfrac{1}{|V|}. \tag{16}$$

Note that for $n = 0$, there is only one component $m = 0$, so that

$$\boldsymbol{k}_{0,0} = \boldsymbol{0} \text{ and } \alpha_{0,0} = \sqrt{\lambda}. \tag{17}$$

The distribution of the wave vectors on a lattice is reflected by Eq. (13) for both the rectangular cuboid and the isosceles right triangular right prism (in which case $L_1 = L_2 = L$), and

Eq. (16) can be directly derived from Eq. (12) in the case of the rectangular cuboid. Indeed, Eq. (12) shows that

$$\forall m,\ \alpha_{n,m} = \sqrt{\frac{2^{\delta_{n_1,0}+\delta_{n_2,0}+\delta_{n_3,0}}}{8|V|}}, \tag{18}$$

where the natural number n corresponds to the triplet $(|n_1|, |n_2|, |n_3|)$, and for every n, the integer m corresponds to the $\frac{8}{2^{\delta_{n_1,0}+\delta_{n_2,0}+\delta_{n_3,0}}}$ possible values of the triplet $(\mathrm{sign}(n_1), \mathrm{sign}(n_2), \mathrm{sign}(n_3))$, which finally proves Eq. (16). In addition, we have the following result, which generalizes the 2D case (Amar *et al.*, 1991): there is a polyhedron P made of V and a few reflections of V, which is a parallelogrammatic right prism, which strictly tessellates the 3D space, and which is such that every eigenfunction ϕ_n is periodic of primitive unit cell P. Then the uniform probability density function on P, $p(\boldsymbol{u}) = \frac{1}{|P|}\mathbf{1}_P(\boldsymbol{u})$, satisfies the following property: the characteristic function $\widehat{p}(\boldsymbol{k})$, defined as the 3D Fourier transform (Eq. (2)) of p, is such that $\forall Q \in \mathbb{N}^*$,

$$\widehat{p}\left(\sum_{q=1}^{Q} \boldsymbol{k}_{n_q,m_q}\right) = 0 \tag{19}$$

for all wave vectors $\boldsymbol{k}_{n_1,m_1} \dots \boldsymbol{k}_{n_Q,m_Q}$ such that $\sum_{q=1}^{Q} \boldsymbol{k}_{n_q,m_q} \neq \mathbf{0}$. In particular, the polyhedron P can be $[0, 2L_1] \times [0, 2L_2] \times [0, 2L_3]$ for both the rectangular cuboid and the isosceles right triangular right prism (in which case $L = L_1 = L_2$). Moreover, the B-function is also periodic of primitive unit cell P, as represented in Fig. 2 in the 2D-case.

4.4. Robin's boundary condition

We still consider a simply connected domain $V \subsetneq \mathbb{R}^3$, whose boundary ∂V is a Lipschitz continuous 2D manifold. Now, the boundary ∂V is characterized by the *specific admittance* $\widehat{\beta}(\boldsymbol{x}, k) \in \mathbb{C}$, which is an essentially bounded function of the position $\boldsymbol{x} \in \partial V$. Then the boundary condition of the Helmholtz equation is

$$\forall \boldsymbol{x} \in \partial V,\ \frac{\partial \varphi(\boldsymbol{x}, k)}{\partial \boldsymbol{n}(\boldsymbol{x})} + 2\imath\pi k \widehat{\beta}(\boldsymbol{x}, k)\varphi(\boldsymbol{x}, k) = 0. \tag{20}$$

In the case of *non-rigid* surfaces, which absorb a part of the energy of the incident wave, $\widehat{\beta}(\boldsymbol{x}, k)$ is complex and the real part of $\widehat{\beta}(\boldsymbol{x}, k)$ is positive. However, when there is no energy absorption, $\widehat{\beta}(\boldsymbol{x}, k)$ is purely imaginary. Also note that when $k = 0$, Eq. (20) reduces to Neumann's boundary condition (Eq. (8)). Since the boundary condition in Eq. (20) explicitly depends on k, the solutions of the homogeneous Helmholtz equation also depend on k, thus Eq. (4) has to be rewritten

$$\Delta\varphi(\boldsymbol{x}, k) + 4\pi^2\kappa(k)^2\varphi(\boldsymbol{x}, k) = 0, \tag{21}$$

where the wave number is now denoted $\kappa(k) \in \mathbb{C}$.

4.4.1. Simply connected bounded domain

If V is a bounded domain, then the set of eigenvalues $\kappa_n(k)$ and eigenfunctions $\varphi_n(\boldsymbol{x},k)$, which are solutions to Eqs. (20) and (21), is still discrete and indexed by $n \in \mathbb{N}$. Moreover, when $k \neq 0$, if there is energy absorption at the boundary (i.e. if $\widehat{\beta}(\boldsymbol{x},k)$ is complex and $\mathrm{Re}(\widehat{\beta}(\boldsymbol{x},k)) > 0$), then both $\kappa_n(k)$ and $\varphi_n(\boldsymbol{x},k)$ are complex and $\mathrm{Im}(\kappa_n(k)) > 0$. However, if there is no energy absorption (i.e. if $\widehat{\beta}(\boldsymbol{x},k)$ is purely imaginary), then $\kappa_n(k)$ and $\varphi_n(\boldsymbol{x},k)$ are real-valued.

4.4.2. Special polyhedra

With the special polyhedra, the situation is different from the Neumann's case. Indeed, in 2D, the isosceles right triangle and the hemiequilateral triangle are no longer solvable in closed-form, so neither are the corresponding right prisms illustrated in Fig. 1. Nevertheless, the rectangle and the equilateral triangle are still solvable in closed-form, provided that function $\boldsymbol{x} \mapsto \widehat{\beta}(\boldsymbol{x},k)$ is constant on every side of the polygon (for instance the latter was addressed in McCartin (2004)), and so are the corresponding right prisms. In this section, we will focus on the particular case of the rectangular cuboid (Kuttruff, 2014, Chap. 3), for the same reasons as explained in Sec. 4.3.2.

So, let us consider again a rectangular cuboid of dimensions L_1, L_2, L_3, so that $V=(0,L_1)\times(0,L_2)\times(0,L_3)$. Let us assume that $\widehat{\beta}(\boldsymbol{x},k) = \widehat{\beta}_{-l}(k) \in \mathbb{C}$ on the face orthogonal to axis $l \in \{1,2,3\}$ and going through $x_l = 0$, and $\widehat{\beta}(\boldsymbol{x},k) = \widehat{\beta}_{+l}(k) \in \mathbb{C}$ on the face orthogonal to axis l and going through $x_l = L_l$. Then the eigenfunctions of the Helmholtz equation (21) can be factorized as

$$\varphi_n(\boldsymbol{x},k) = \prod_{l=1}^{3} \varphi_{n,l}(x_l,k), \tag{22}$$

where $\forall l \in \{1,2,3\}$, function $\varphi_{n,l}$ is of the form

$$\varphi_{n,l}(x_l,k) = a_{n,l}(k)e^{-2\imath\pi\kappa_{n,l}(k)x_l} + b_{n,l}(k)e^{2\imath\pi\kappa_{n,l}(k)x_l}, \tag{23}$$

with $a_{n,l}(k)$, $b_{n,l}(k)$ and $\kappa_{n,l}(k) \in \mathbb{C}$. Indeed, the eigenfunctions $\varphi_n(\boldsymbol{x},k)$ in Eq. (22) are clearly solutions to the Helmholtz equation (21), associated with the eigenvalues

$$\kappa_n(k) = \sqrt{\kappa_{n,1}(k)^2 + \kappa_{n,2}(k)^2 + \kappa_{n,3}(k)^2}.$$

Moreover, at the cuboid boundaries, Robin's boundary condition (Eq. (20)) yields $\dot{\varphi}_{n,l}(0,k) = 2\imath\pi k\widehat{\beta}_{-l}(k)\varphi_{n,l}(0,k)$ at $x_l = 0$, and $\dot{\varphi}_{n,l}(L_l,k) = -2\imath\pi k\widehat{\beta}_{+l}(k)\varphi_{n,l}(L_l,k)$ at $x_l = L_l$, which can be written as a 2×2 linear system of equations:

$$\boldsymbol{K}\begin{bmatrix} a_{n,l}(k) \\ b_{n,l}(k) \end{bmatrix} = \begin{bmatrix} 0 \\ 0 \end{bmatrix},$$

where $\boldsymbol{K}$ is the 2×2 matrix

$$\begin{bmatrix} \kappa_{n,l}(k) + k\widehat{\beta}_{-l}(k) & -\kappa_{n,l}(k) + k\widehat{\beta}_{-l}(k) \\ (-\kappa_{n,l}(k) + k\widehat{\beta}_{+l}(k))e^{-2\imath\pi\kappa_{n,l}(k)L_l} & (\kappa_{n,l}(k) + k\widehat{\beta}_{+l}(k))e^{2\imath\pi\kappa_{n,l}(k)L_l} \end{bmatrix}.$$

For a non-zero solution $(a_{n,l}(k), b_{n,l}(k))$ to exist, the determinant of this system has to be zero, thus

$$\frac{\Big(\kappa_{n,l}(k) - k\widehat{\beta}_{-l}(k)\Big)\Big(\kappa_{n,l}(k) - k\widehat{\beta}_{+l}(k)\Big)}{\Big(\kappa_{n,l}(k) + k\widehat{\beta}_{-l}(k)\Big)\Big(\kappa_{n,l}(k) + k\widehat{\beta}_{+l}(k)\Big)} = e^{4\imath\pi\kappa_{n,l}(k)L_l}. \tag{24}$$

The solutions $\kappa_{n,l}(k)$ of Eq. (24) cannot be expressed in closed-form and have to be computed numerically (Kuttruff, 2014, Chap. 3). Note that the squared magnitude of function $\varphi_{n,l}(x_l, k)$ defined in Eq. (23) is represented in Kuttruff (2014, Fig. 3.5 p. 82) for $n = 4$ and for various values of $\widehat{\beta}_{\pm l}(k)$, in order to illustrate the distortion of the normal modes induced by a non-zero specific admittance.

5. Fundamentals of the statistical wave field theory

In Badeau (2024, Sec. IV), we introduced the three mathematical assumptions of the version of the statistical wave field theory dedicated to mixing billiards:

- Assumption 1: the source's position is a random variable uniformly distributed in V;
- Assumption 2: the frequency f (or equivalently the wave number k) is large;
- Assumption 3: the mean and covariances of the B-function are stationary and isotropic.

We showed that Assumptions 1 and 3 were directly related to the mixing property, and Assumption 2 permitted us to locally approximate a possibly curved boundary surface by its tangent plane. The three assumptions were sorted in this particular order because this was the only possible deductive way of deriving the mathematical equations of the theory. In this paper, the situation is different, because we no longer consider mixing billiards, but instead we focus on the special polyhedra, and we only address the Neumann's case. In particular, Assumption 2 is no longer required, and indeed the theory predictions will hold right from the zero frequency. In other respects, the special polyhedra are neither mixing nor ergodic, yet almost every ray trajectory still explores space in an ergodic manner (i.e. uniformly over time), as explained in Sec. 3. Consequently, a relaxed version of Assumption 3 holds (Sec. 5.1): the mean and covariances of the B-function are still stationary [as can be noticed in Fig. 2, the B-function is actually a periodic, and thus stationary, simple point process, as defined in Daley and Vere-Jones (2003, Chap. 8)], but no longer isotropic (as can be noticed *e.g.* in Fig. 2(a), the atoms are spatially distributed along straight lines whose directions are parallel to the sides of the rectangle). Finally, Assumption 1 no longer holds in the strict sense because, even though space is still explored in an ergodic manner, it is not explored in a mixing manner (in the sense that two parallel ray trajectories starting at close spatial positions will almost surely stay parallel and close to each other), so the stationary statistics of the wide-sense stationary (WSS) B-function do depend on the source's position. Nevertheless, we will show that when the power spectrum of the B-function is smoothed over frequency, the resulting auto-covariance function (ACF) becomes independent again of the source's position (Sec. 5.2). In this way, Assumption 1 still holds in a broader sense.

5.1. Stationarity of the B-function

The first assumption considered here is simply related to the periodicity of the B-function, which is clearly visible in Fig. 2: *The mean and covariances of the B-function are stationary.* This assumption is enforced by introducing a random translation of space, characterized by the probability density function p introduced in Sec. 4.3.2. We thus consider the random process $B(\boldsymbol{y}-\boldsymbol{u},\boldsymbol{x}_0)$, where $\boldsymbol{u}$ is a random vector with probability distribution p, and we will show that it is WSS. First, substituting Eq. (14) into Eq. (11) yields $B(\boldsymbol{y},\boldsymbol{x}_0) = \sum_{n\in\mathbb{N}} B_n(\boldsymbol{y},\boldsymbol{x}_0)$, where

$$B_n(\boldsymbol{y},\boldsymbol{x}_0) = \sum_{m_0}\sum_{m} \alpha_{n,m_0}\,\alpha_{n,m}\,e^{2\imath\pi\boldsymbol{k}_{n,m_0}^\top\boldsymbol{x}_0}\,e^{2\imath\pi\boldsymbol{k}_{n,m}^\top\boldsymbol{y}}.$$

Then Eq. (19) with $Q=1$ and Eq. (17) yield $\mathbb{E}\left[B_n(\boldsymbol{y}-\boldsymbol{u},\boldsymbol{x}_0)\right] = \lambda\,\delta_{n,0}$, which shows that the B-function is first order stationary, of mean $\mu_B = \lambda$. In the same way, Eq. (19) with $Q=2$ and Eq. (15) show that $\forall n_1, n_2 > 0$,

$$\mathrm{cov}[B_{n_1}(\boldsymbol{y}_1-\boldsymbol{u},\boldsymbol{x}_0), B_{n_2}(\boldsymbol{y}_2-\boldsymbol{u},\boldsymbol{x}_0)] = \delta_{n_1,n_2}\,\lambda_n(\boldsymbol{x}_0)\sum_m |\alpha_{n,m}|^2\; e^{2\imath\pi\boldsymbol{k}_{n,m}^\top(\boldsymbol{y}_1-\boldsymbol{y}_2)} \tag{25}$$

where

$$\lambda_n(\boldsymbol{x}_0) \triangleq \sum_{m_1}\sum_{m_2} \alpha_{n,m_1}\overline{\alpha_{n,m_2}}\,e^{2\imath\pi(\boldsymbol{k}_{n,m_1}-\boldsymbol{k}_{n,m_2})^\top\boldsymbol{x}_0}. \tag{26}$$

Eq. (25) shows that the B-function is WSS, of ACF

$$\begin{array}{rcl}\Gamma_B^0(\boldsymbol{z};\boldsymbol{x}_0) \triangleq & \mathrm{cov}[B(\boldsymbol{y}+\boldsymbol{z}-\boldsymbol{u},\boldsymbol{x}_0), B(\boldsymbol{y}-\boldsymbol{u},\boldsymbol{x}_0)] \\ = & \sum_{n\in\mathbb{N}^*}\lambda_n(\boldsymbol{x}_0)\sum_m |\alpha_{n,m}|^2\; e^{2\imath\pi\boldsymbol{k}_{n,m}^\top\boldsymbol{z}}.\end{array} \tag{27}$$

It can be noticed that $\Gamma_B^0(\boldsymbol{z};\boldsymbol{x}_0)$ explicitly depends on the original source position $\boldsymbol{x}_0$, which is in agreement with the fact that space is not explored in a mixing manner. Moreover, it can also be noticed that function $n \mapsto \lambda_n(\boldsymbol{x}_0)$ is oscillating around a value that can be calculated by averaging $\lambda_n(\boldsymbol{x}_0)$ over $\boldsymbol{x}_0$. Indeed, Eqs. (26), (19) with $Q=2$, (15) and (16) yield

$$\int \lambda_n(\boldsymbol{x}_0)p(\boldsymbol{x}_0)d\boldsymbol{x}_0 = \sum_m |\alpha_{n,m}|^2 = \lambda.$$

5.2. Random source position

Since the statistical wave field theory involves a power spectrum that is smoothed over the wave numbers k_n, replacing $\lambda_n(\boldsymbol{x}_0)$ by its average value λ in Eq. (27) will not affect the smoothed power spectrum. Therefore, it is still possible to assume that *the source position $\boldsymbol{x}_0$ is randomly and uniformly distributed in V*, even though space is not explored in a mixing manner. Consequently, the B-function is WSS, of same mean $\mu_B = \lambda$, and ACF

$$\Gamma_B^0(\boldsymbol{z}) = \lambda\sum_{n\in\mathbb{N}^*}\sum_m |\alpha_{n,m}|^2\; e^{2\imath\pi\boldsymbol{k}_{n,m}^\top\boldsymbol{z}}. \tag{28}$$

6. Special theory (Neumann's boundary condition)

In the case of Neumann's boundary condition, the B-function is WSS, as explained in Sec. 5, so the room response to a punctual source is WSS over both space and time, and it can be decomposed on the set of plane waves $e^{2\imath\pi \boldsymbol{k}^\top \boldsymbol{x}} \cos(2\pi c \|\boldsymbol{k}\|_2 t)$ for all wave vectors $\boldsymbol{k} \in \mathbb{R}^3$ [as in Eq. (87) in Badeau (2024)]. Then the purpose of the special statistical wave field theory is to calculate the spectral measure $\widehat{\Gamma}_B(\boldsymbol{k})$, which can be interpreted as the power distribution of the plane waves in this decomposition.

As in Sec. 4.3.2, we first focus on the rectangular cuboid (Sec. 6.1), before addressing the general case of special polyhedra (Sec. 6.2).

6.1. Rectangular cuboid

Let us consider a rectangular cuboid of dimensions L_1, L_2, L_3, so that $V = (0, L_1) \times (0, L_2) \times (0, L_3)$ as in Sec. 4.3.2. By substituting Eqs. (13) and (18) into Eq. (28), where the natural number n corresponds to the triplet $(|n_1|, |n_2|, |n_3|)$, and for every n, the integer m corresponds to the $\frac{8}{2^{\delta_{n_1,0}+\delta_{n_2,0}+\delta_{n_3,0}}}$ possible values of the triplet $(\mathrm{sign}(n_1), \mathrm{sign}(n_2), \mathrm{sign}(n_3))$, we obtain

$$\Gamma_B^0(\boldsymbol{z}) = \lambda \prod_{l=1}^{3} \mathrm{III}_{2L_l}(z_l) + \tfrac{\lambda^2}{2} \sum_{l=1}^{3} \prod_{l' \neq l} L_{l'} \mathrm{III}_{2L_{l'}}(z_{l'}) + \tfrac{\lambda^2}{4} \sum_{l=1}^{3} L_l \mathrm{III}_{2L_l}(z_l) - \tfrac{7}{8}\lambda^2 \tag{29}$$

whose 3D Fourier transform (Eq. (2)) is

$$\widehat{\Gamma}_B^0(\boldsymbol{k}) = \tfrac{\lambda^2}{8} \left(\prod_{l=1}^{3} \mathrm{III}_{\frac{1}{2L_l}}(k_l) + \sum_{l=1}^{3} \delta(k_l) \prod_{l' \neq l} \mathrm{III}_{\frac{1}{2L_{l'}}}(k_{l'}) + \sum_{l=1}^{3} \mathrm{III}_{\frac{1}{2L_l}}(k_l) \prod_{l' \neq l} \delta(k_{l'})) - 7\delta(\boldsymbol{k}) \right). \tag{30}$$

The second order measure $M_B^0(\boldsymbol{z}) \triangleq \Gamma_B^0(\boldsymbol{z}) + \lambda^2$ is represented in 2D in Fig. 3(a): it is made of atoms located on a rectangular Bravais lattice, of horizontal and vertical lines going through these atoms, and of a constant term represented by the colored background. Note that Fig. 3(a) represents the second order measure $M_B^0(\boldsymbol{z})$ rather than the ACF $\Gamma_B^0(\boldsymbol{z})$ mainly for visualization purposes, in order to avoid representing negative terms such as $-\frac{7}{8}\lambda^2$ in Eq. (29) (the same remark will apply to Figs. 3(b) and (d)). The 3D Fourier transform of $M_B^0(\boldsymbol{z})$, the raised spectral measure $\widehat{M}_B^0(\boldsymbol{k}) \triangleq \widehat{\Gamma}_B^0(\boldsymbol{k}) + \lambda^2 \delta(\boldsymbol{k})$, is illustrated in 2D in Fig. 3(c): it is discrete, i.e. made only of atoms that are also located on a rectangular Bravais lattice (the different sizes of the points are intended to represent the different powers of the atoms, according to Eq. (28)).

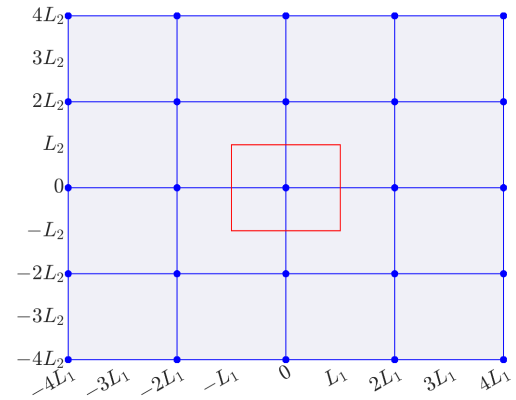

(a) Exact second order measure $M_B^0(\boldsymbol{z}) = \Gamma_B^0(\boldsymbol{z}) + \lambda^2$

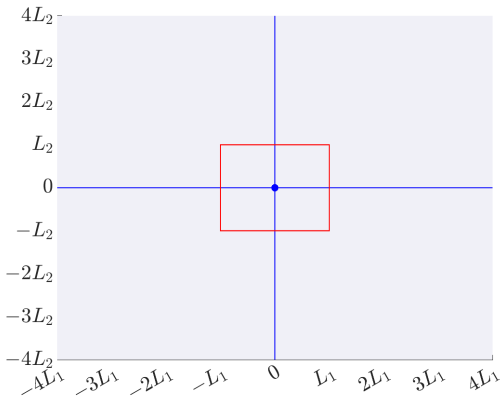

(b) Reduced second order measure $M_B(\boldsymbol{z}) = \Gamma_B(\boldsymbol{z}) + \lambda^2$ (equal to $M_B^0(\boldsymbol{z})$ inside the red frame)

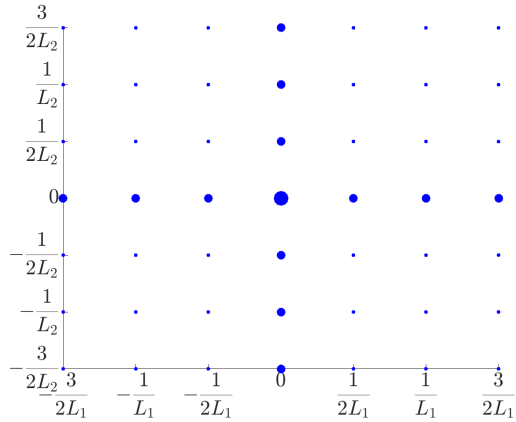

(c) Discrete raised spectral measure $\widehat{M}_B^0(\boldsymbol{k}) = \widehat{\Gamma}_B^0(\boldsymbol{k}) + \lambda^2\delta(\boldsymbol{k})$ (the different sizes of the points represent different powers)

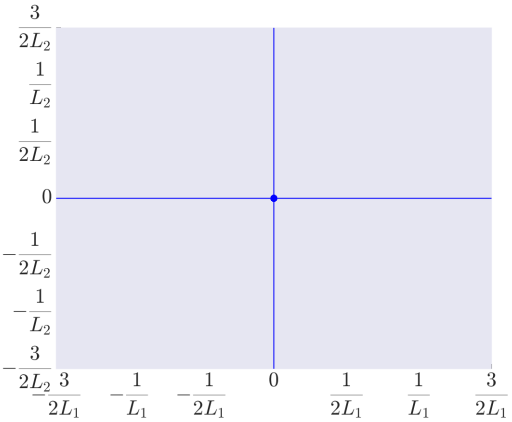

(d) Reduced raised spectral measure $\widehat{M}_B(\boldsymbol{k}) = \widehat{\Gamma}_B(\boldsymbol{k}) + \lambda^2\delta(\boldsymbol{k})$ (each line is parallel to each set of parallel lines in Fig. 2(a))

Figure 3: Second order measures and raised spectral measures of the rectangle

As previously explained, the statistical wave field theory rather focuses on smoothed power spectra. Here spectral smoothing can be achieved by modifying the expression of the ACF in Eq. (29) by keeping only the terms that are non-zero in the vicinity of $\boldsymbol{z} = 0$:

$$\Gamma_B(\boldsymbol{z}) = \lambda\delta(\boldsymbol{z}) + \tfrac{\lambda^2}{2}\sum_{l=1}^{3}\prod_{l'\neq l} L_{l'}\delta(z_{l'}) + \tfrac{\lambda^2}{4}\sum_{l=1}^{3} L_l\delta(z_l) - \tfrac{7}{8}\lambda^2. \tag{31}$$

The resulting reduced second order measure $M_B(\boldsymbol{z}) = \Gamma_B(\boldsymbol{z}) + \lambda^2$ is represented in 2D in Fig. 3(b). It can be noticed that it is equal to the exact second order measure inside the region bounded by the red frame in Figs. 3(a) and (b), so that multiplying either of these two measures by the indicator function of this region would produce the same result. Note that

this particular region is made of all vectors $\boldsymbol{z} = \boldsymbol{x}_1 - \boldsymbol{x}_2$ for $\boldsymbol{x}_1, \boldsymbol{x}_2 \in V$, so it characterizes all possible pairs of points where the correlations of the wave field can be practically estimated from experimental measurements inside the room volume. Also note that multiplication in the space domain by this indicator function is equivalent to convolution in the spectral domain by its 3D Fourier transform, which acts as a smoothing filter.

The 3D Fourier transform of the reduced ACF in Eq. (31) can be written as $\widehat{\Gamma}_B(\boldsymbol{k}) = \widehat{M}_B(\boldsymbol{k}) - \lambda^2\delta(\boldsymbol{k})$, where the reduced raised spectral measure $\widehat{M}_B(\boldsymbol{k})$ can be decomposed as follows:

$$\begin{array}{rll} \widehat{M}_B(\boldsymbol{k}) = & \lambda & \text{volume term} \\ & +\frac{\lambda^2}{2}\sum_{l=1}^{3}\delta(k_l)\prod_{l'\neq l}L_{l'} & \text{surface term} \\ & +\frac{\lambda^2}{4}\sum_{l=1}^{3}L_l\prod_{l'\neq l}\delta(k_{l'}) & \text{edge term} \\ & +\frac{\lambda^2}{8}\delta(\boldsymbol{k}) & \text{vertex term} \end{array} \tag{32}$$

As the names suggest, the *volume term* is related to the space inside the polyhedron, characterized by its volume $|V|$; the *surface term* is related to its faces, characterized by their areas $\prod_{l'\neq l} L_{l'}$; the *edge term* is related to its edges, characterized by their lengths L_l; and the *vertex term* is related to its vertices. The reduced raised spectral measure in Eq. (32) is illustrated in 2D in Fig. 3(d), where the colored background represents the constant volume term λ. This spectral measure is smoother than the exact (discrete) one in Fig. 3(c), but it is not a smooth function. Anyway, convolving either of these two raised spectral measures by the previously mentioned smoothing filter would produce the same result, which is clearly apparent when comparing Figs. 3(c) and (d).

From now on, we will forget the exact expressions of the ACF in Eq. (29) and of the discrete spectral measure in Eq. (30). Instead, the statistical wave field theory rather focuses on the reduced ACF in Eq. (31) and on its 3D Fourier transform, the reduced spectral measure $\widehat{\Gamma}_B(\boldsymbol{k}) = \widehat{M}_B(\boldsymbol{k}) - \lambda^2\delta(\boldsymbol{k})$ with $\widehat{M}_B(\boldsymbol{k})$ as defined in Eq. (32).

6.2. General case

Let us now address the general case of special polyhedra. First, note that the representation of the raised spectral measure $\widehat{M}_B(\boldsymbol{k})$ of the rectangular cuboid in Fig. 3(d) contains two straight lines, which represent measures supported by the 2D subspaces parallel to the polyhedron's faces, and which are proportional to the 2D Lebesgue measure. These subspaces are also parallel, not only to the polyhedron's faces, but also to the faces of all the successive reflections of this polyhedron, which strictly tessellate the 3D space, as represented in 2D in Fig. 2(a).

Room is missing here to develop the detailed mathematical proofs, but the same remark actually holds for the three other special polyhedra, whose raised spectral measures $\widehat{M}_B(\boldsymbol{k})$ are represented in 2D in Fig. 4. The case of the equilateral triangle (Fig. 4(b)) is similar to that of the rectangular cuboid: each line represents a 2D subspace parallel to one of the polyhedron's faces. However the case of the isosceles right triangle and the hemiequilateral triangle (Figs. 4(a) and (c)) is a bit different: each line represents a 2D subspace that is not necessarily parallel to one of the original polyhedron's faces, but rather to one of the faces of

its *successive reflections*. So, each line represented in Figs. 4(a) and (c) is parallel to each set of parallel lines of the strict space tessellations represented in Fig. 2(b) and (d), respectively.

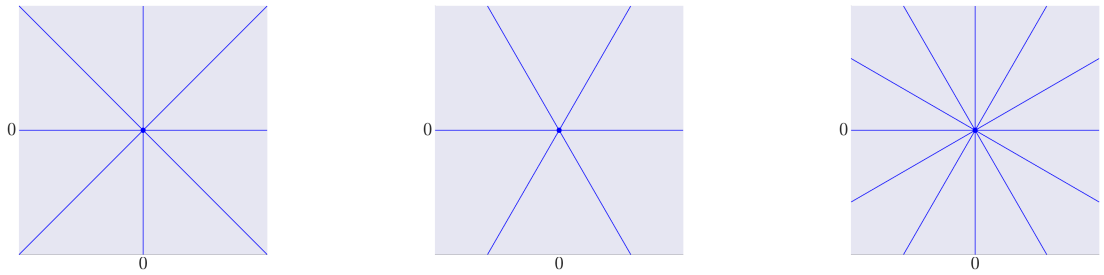

(a) Isosceles right triangle (each line is parallel to each set of parallel lines in Fig. 2(b))

(b) Equilateral triangle (each line is parallel to each set of parallel lines in Fig. 2(c))

(c) Hemiequilateral triangle (each line is parallel to each set of parallel lines in Fig. 2(d))

Figure 4: Reduced raised spectral measures of special polygons

Moreover, note that the four raised spectral measures represented in Figs. 3(d) and 4(a)-(c) present rotational invariances. This is because they are invariant to all successive reflections through the polyhedra's faces. Mathematically, there is actually a one-to-one correspondence between the four special polyhedra and the four non-trivial cyclic crystallographic point groups C_n, as shown in Table 1. In crystallographic notation (Burzlaff and Zimmermann, 2006), C_n denotes the finite group of rotations (of cardinal n) that has an n-fold rotation axis, i.e. that is generated by a unique rotation of angle $\frac{2\pi}{n}$.

Special polyhedron	Crystallographic point group	Angle of the generator
Rectangular cuboid	C_2	π
Isosceles right triangular right prism	C_4	$\frac{\pi}{2}$
Equilateral triangular right prism	C_3	$\frac{2\pi}{3}$
Hemiequilateral triangular right prism	C_6	$\frac{\pi}{3}$

Table 1: Crystallographic point groups associated with the four special polyhedra

So, the raised spectral measure of each special polyhedron is invariant to any rotation $\boldsymbol{R}$ in C_n. Similarly to Eq. (32), the general expression of the raised spectral measure $\widehat{M}_B(\boldsymbol{k})$ can be decomposed as follows:

$$\begin{aligned}
\widehat{M}_B(\boldsymbol{k}) = \; & \lambda && \text{volume term} \\
& + \tfrac{\lambda^2}{4} \sum_f S_f \left(\tfrac{1}{n} \sum_{\boldsymbol{R} \in C_n} \delta(\boldsymbol{n}_f^\top \boldsymbol{R}\, \boldsymbol{k}) \right) && \text{surface term} \\
& + \tfrac{\lambda^2}{24} \sum_e L_e (\tfrac{\pi}{\theta_e} - \tfrac{\theta_e}{\pi}) \left(\tfrac{1}{n} \sum_{\boldsymbol{R} \in C_n} \delta(\boldsymbol{P}_{\boldsymbol{d}_e^\perp}^\top \boldsymbol{R}\, \boldsymbol{k}) \right) && \text{edge term} \\
& + \tfrac{\lambda^2}{96} \sum_v (\tfrac{\pi}{\theta_v} - \tfrac{\theta_v}{\pi})\, \delta(\boldsymbol{k}) && \text{vertex term}
\end{aligned} \tag{33}$$

In Eq. (33), the surface term involves a sum over every face f of the polyhedron, characterized by its area S_f and outward unit normal vector $\boldsymbol{n}_f$. Similarly, the edge term involves a sum over every edge e, characterized by its length L_e, direction vector $\boldsymbol{d}_e$, and angle θ_e between the two faces adjacent to the edge ($\boldsymbol{P}_{\boldsymbol{d}_e^\perp}$ denotes any 3×2 orthonormal matrix whose 2D range space is the orthogonal complement of $\boldsymbol{d}_e$). Finally, the vertex term involves a sum over every vertex v, characterized by the angle θ_v between two of its three adjacent faces (the two other angles are equal to $\frac{\pi}{2}$, since all special polyhedra are right prisms). It can be easily verified that Eq. (33) reduces to Eq. (32) in the particular case of the rectangular cuboid.

7. General theory (Robin's boundary condition)

The main purpose of the general statistical wave field theory is to show that Robin's boundary condition induces a non-linear distortion of the real wave vectors $\boldsymbol{k}$ related to Neumann's boundary condition. In particular, when there is energy absorption at the boundary (i.e. when $\mathrm{Re}(\widehat{\beta}(k)) > 0$), the distorted Robin's wave vectors $\boldsymbol{\kappa}$ are complex, and similarly to the Neumann case addressed at the beginning of Sec. 6, the room response to a punctual source can be decomposed on a set of plane waves $e^{2\imath\pi\left(\boldsymbol{\kappa}^\top \boldsymbol{x} + c\sqrt{\boldsymbol{\kappa}^\top\boldsymbol{\kappa}}\, t\right)}$ and $e^{2\imath\pi\left(\overline{\boldsymbol{\kappa}}^\top \boldsymbol{x} - c\overline{\sqrt{\boldsymbol{\kappa}^\top\boldsymbol{\kappa}}}\, t\right)}$, where $\sqrt{\boldsymbol{\kappa}^\top\boldsymbol{\kappa}}$ denotes the complex square root of $\boldsymbol{\kappa}^\top\boldsymbol{\kappa} \in \mathbb{C}$ with positive imaginary part (these plane waves have direction $\mathrm{Re}(\boldsymbol{\kappa})$, frequencies $\pm c\,\mathrm{Re}(\sqrt{\boldsymbol{\kappa}^\top\boldsymbol{\kappa}})$ and temporal attenuation coefficient $c\,\mathrm{Im}(\sqrt{\boldsymbol{\kappa}^\top\boldsymbol{\kappa}}) > 0$). In addition, the general statistical wave field theory provides the closed-form expression of the non-linear distortion that transforms the Neumann's wave vectors $\boldsymbol{k}$ into the corresponding Robin's wave vectors $\boldsymbol{\kappa}$.

In the case of mixing billiards that we adressed in Badeau (2024, Sec. VI), this non-linear distortion is isotropic, and we were able to identify it by using a complex mathematical approach based on a change of variable that relates Neumann's power spectrum to Robin's pseudo spectrum. Here, in the case of special polyhedra, the non-linear distortion is anisotropic, and its identification is much easier, since the expression of the wave vectors is available in closed-form.

As in Sec. 4.4, we first focus on the rectangular cuboid (Sec. 7.1), before addressing the general case of special polyhedra (Secs. 7.2 and 7.3).

7.1. Rectangular cuboid

The wave vectors of the rectangular cuboid are indexed by three integers $(n_1, n_2, n_3) \in \mathbb{Z}^3$:

$$\boldsymbol{\kappa}_{n_1,n_2,n_3}(k) = \begin{bmatrix} \mathrm{sign}(n_1)\kappa_{|n_1|,1}(k) \\ \mathrm{sign}(n_2)\kappa_{|n_2|,2}(k) \\ \mathrm{sign}(n_3)\kappa_{|n_3|,3}(k) \end{bmatrix}, \tag{34}$$

where the coefficients $\kappa_{n,l}(k)$ are the solutions to Eq. (24). These solutions can be rewritten in the following implicit form:

$$\kappa_{n,l}(k) = k_{n,l} + \imath\tfrac{\lambda S_l}{4\pi}\left(\ln\left(\tfrac{\kappa_{n,l}(k)+k\widehat{\beta}_{-l}(k)}{\kappa_{n,l}(k)-k\widehat{\beta}_{-l}(k)}\right) + \ln\left(\tfrac{\kappa_{n,l}(k)+k\widehat{\beta}_{+l}(k)}{\kappa_{n,l}(k)-k\widehat{\beta}_{+l}(k)}\right)\right), \tag{35}$$

where $k_{n,l} = \frac{n}{2L_l}$, $\lambda = \frac{1}{|V|} = \frac{1}{L_1 L_2 L_3}$, and $S_l = \frac{1}{\lambda L_l}$ is the surface area of the faces orthogonal to axis l. Equation (35) explicitly shows how the complex wave vectors $\boldsymbol{\kappa}_{n_1,n_2,n_3}(k)$ of Robin's boundary condition are related to the real wave vectors $\boldsymbol{k}_{n_1,n_2,n_3} = [k_{n,1}, k_{n,2}, k_{n,3}]^\top$ of Neumann's boundary condition.

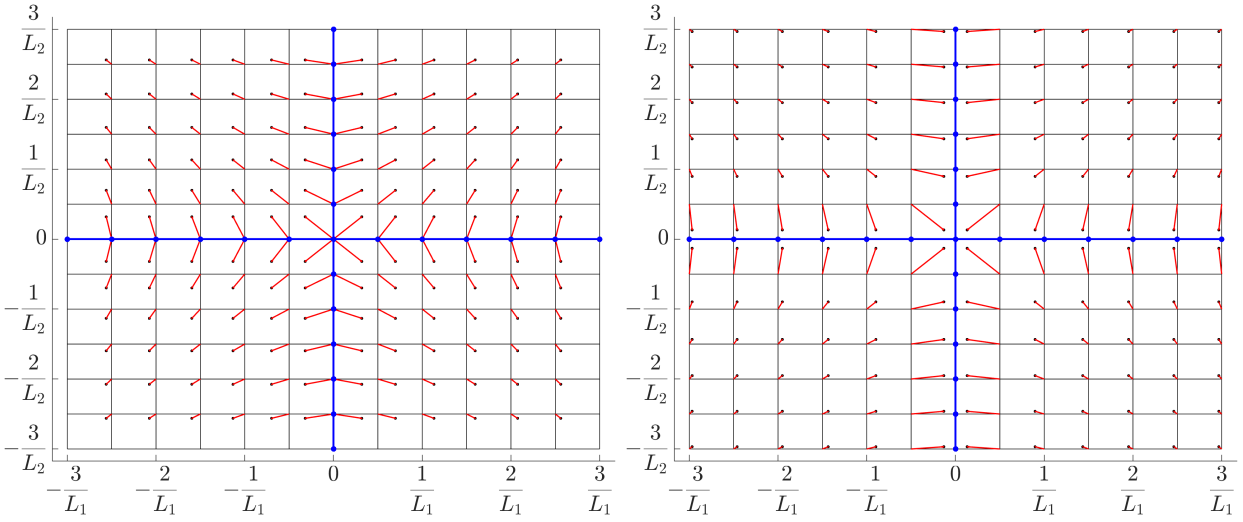

(a) Rectangle ($\widehat{\beta}(k) \in -\imath\mathbb{R}_+$, same blue lines as in Fig. 3(d), which are repulsors)

(b) Rectangle ($\widehat{\beta}(k) \in +\imath\mathbb{R}_+$, same blue lines as in Fig. 3(d), which are attractors)

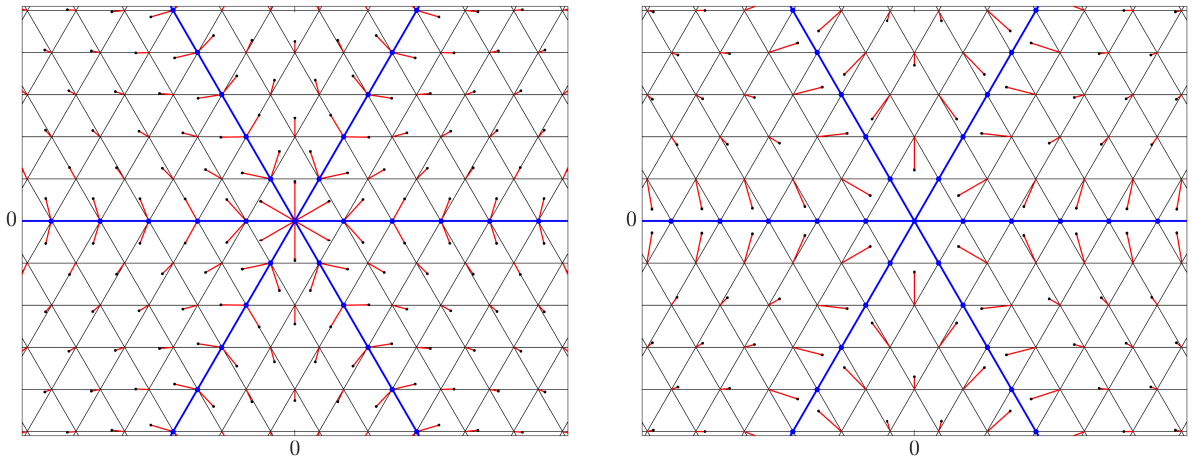

(c) Equilateral triangle ($\widehat{\beta}(k) \in -\imath\mathbb{R}_+$, same blue lines as in Fig. 4(b), which are repulsors)

(d) Equilateral triangle ($\widehat{\beta}(k) \in +\imath\mathbb{R}_+$, same blue lines as in Fig. 4(b), which are attractors)

Figure 5: Wave vectors distortion in 2D (Neumann's wave vectors located at vertices of the black grid, Robin's wave vectors located at black points, red arrows pointing from the former to the latter)

The wave vectors of the rectangular cuboid are represented in 2D in Figs. 5(a) and (b), in the case of a single value $\widehat{\beta}_{\pm l}(k) \triangleq \widehat{\beta}(k)$ that is purely imaginary, thus the wave vectors $\boldsymbol{\kappa}_{n_1,n_2,n_3}(k)$ are real-valued. In both figures, each wave vector $\boldsymbol{k}_{n_1,n_2,n_3}$ of Neumann's bound-

ary condition is located at a vertex of the black rectangular grid, whereas each wave vector $\boldsymbol{\kappa}_{n_1,n_2,n_3}(k)$ of Robin's boundary condition is located at a black point, and red arrows point from the former to the latter, so as to highlight the nonlinear distortion of the wave vector space, which is clearly anisotropic. In the case $\mathrm{Im}(\widehat{\beta}(k)) < 0$ that is represented in Fig. 5(a), note that the wave vectors of Neumann's boundary condition that are located on the same blue lines as in Fig. 3(d) (represented by blue dots), except for the one located at the origin, are divided into two wave vectors of Robin's boundary condition, which are moved to the two different half spaces separated by this line. On the whole, the 2D subspaces represented by these blue lines, which are parallel to the polyhedron's faces, seem to act as repulsors, which drive the wave vectors away. This effect corresponds to a mass-controlled boundary surface, as explained in Kuttruff (2014, p. 81). On the contrary, in the case $\mathrm{Im}(\widehat{\beta}(k)) > 0$ that is represented in Fig. 5(b), the blue lines seem to act as attractors, which bring the wave vectors closer. This effect corresponds to a compliance boundary surface, i.e. a surface with the impedance of a spring, as explained in Kuttruff (2014, p. 81). The case of the wave vectors of Neumann's boundary condition that are located on the blue lines (represented by blue dots) is especially interesting: the distortion of the wave vector space makes them disappear in a singularity (in a mathematical sense that will be defined hereunder), along with the power $\lambda \left|\alpha_{n,m}\right|^2$ they carry (see Eq. (28)). This is related to the fact that $\forall l \in \{1,2,3\}$, Eq. (35) does not admit any real solution for $n = 0$ and $k \neq 0$.

Let us now investigate the case of a complex value $\widehat{\beta}(k)$ with positive real part (which means that the boundary surface absorbs a part of the energy of the incident wave), so that the Robin's wave vectors $\boldsymbol{\kappa}(k)$ are complex-valued. For visualization purpose, we will no longer consider discrete, but rather continuous values of both coordinates k_l and $\kappa_l(k)$ (so the index n disappears). Figure 6 then represents the variations of a single coordinate $\kappa_l(k)$ as a function of the parameter $k_l \in \mathbb{R}$, which is defined as in Eq. (35), for a single value $\widehat{\beta}(k)$: $\kappa_l(k) = k_l + \imath \frac{\lambda S_l}{2\pi} \ln\left(\frac{\kappa_l(k)+k\widehat{\beta}(k)}{\kappa_l(k)-k\widehat{\beta}(k)}\right)$. Note that this equation defines $\kappa_l(k)$ implicitly, and it may happen that there is not a single solution $\kappa_l(k)$ for all values of $k_l \in \mathbb{R}$. So, the domain $\mathbb{K}$ of the function $k_l \mapsto \kappa_l(k)$ may not be $\mathbb{R}$, and the set $\mathbb{R}\backslash\mathbb{K}$ where this function is not defined will be referred to as a *singularity*, which is a common meaning of this word in mathematics.

In Fig. 6, the x-axis represents the real part of complex numbers, and the y-axis their imaginary part. Since k_l is real, its values (represented in magenta) belong to the x-axis, whereas $\kappa_l(k)$ is complex, thus its values (represented in blue) form a curve in the complex plane. As in Figs. 5(a) and (b), red arrows point from the values k_l to the corresponding values $\kappa_l(k)$, so as to highlight the nonlinear distortion of the wave vector space. In Fig. 6(a), $\mathrm{Im}(\widehat{\beta}(k)) < 0$, so the y-axis seems to act as a repulsor that drives the wave vectors away, as in Fig. 5(a). Note that there is a gap in the set of values of $\mathrm{Re}(\kappa_l(k))$, which corresponds to the space between the two dotted vertical blue lines in Fig. 6(a). Therefore the set of values $\kappa_l(k)$ is disconnected (it forms two separate blue curves). In Fig. 6(b), $\mathrm{Im}(\widehat{\beta}(k)) > 0$, so the y-axis seems to act as an attractor that brings the wave vectors closer, as in Fig. 5(b). Again, there is a gap in the set of values of $\mathrm{Re}(\kappa_l(k))$, which corresponds to the space between the two dotted vertical blue lines in Fig. 6(b). Therefore the set of values $\kappa_l(k)$ is also disconnected. In addition, note that the values of k_l in the interval $(-\frac{1}{2L_l}, \frac{1}{2L_l})$ (represented by the black

line segment on the x-axis) do not belong to the domain $\mathbb{K}$. So, this interval represents a *singularity* of function $k_l \mapsto \kappa_l(k)$, in the mathematical sense that we defined above. This singularity can be interpreted as a "black hole" since, as previously noticed from Fig. 5(b), the power carried by the wave vectors located in this particular region of Neumann's wave vector space disappears in the distorted Robin's wave vectors space [be aware that this kind of "black hole" should not to be confused with the notion of *acoustic black holes* in structures (Pelat *et al.*, 2020)].

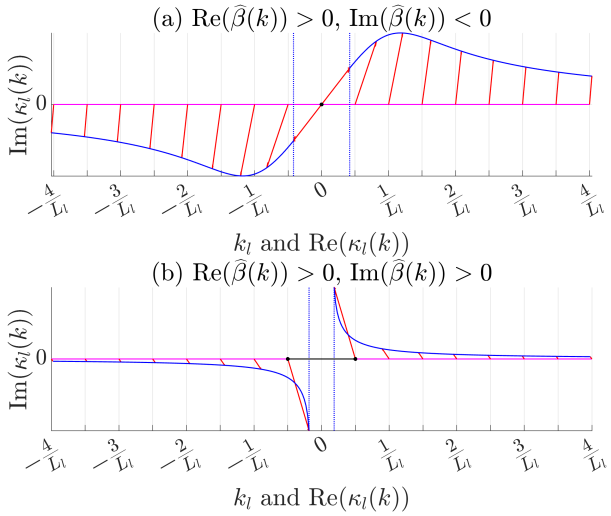

Figure 6: Wave vectors distortion in 1D (Neumann's wave vectors in magenta, Robin's wave vectors in blue, red arrows pointing from the former to the later, singularity as a black line segment)

7.2. General case (in the strict sense)

As already mentioned in Sec. 4.4.2, only the rectangular cuboid and the equilateral triangular right prism are solvable in closed-form in the case of Robin's boundary condition. So, strictly speaking, the "general case" that is referred to in this section actually includes only these two special polyhedra. In both cases, the wave vectors distortion admits the following implicit closed-form expression:

$$\boldsymbol{\mathcal{K}}(\boldsymbol{k},k) = \boldsymbol{k} + \tfrac{\imath\lambda}{4\pi} \sum_f S_f \ln\left(\frac{\boldsymbol{n}_f^\top \boldsymbol{\mathcal{K}}(\boldsymbol{k},k) + k\,\widehat{\beta}_f(k)}{\boldsymbol{n}_f^\top \boldsymbol{\mathcal{K}}(\boldsymbol{k},k) - k\,\widehat{\beta}_f(k)} \right) \boldsymbol{n}_f, \tag{36}$$

which indeed yields $\boldsymbol{\mathcal{K}}(\boldsymbol{k}_{n_1,n_2,n_3},k) = \boldsymbol{\kappa}_{n_1,n_2,n_3}(k)$ in the case of the rectangular cuboid, where $\boldsymbol{k}_{n_1,n_2,n_3}$ was defined in Eq. (13) and $\boldsymbol{\kappa}_{n_1,n_2,n_3}(k)$ was defined in Eqs. (34) and (35). Similarly to the expression of the raised spectral measure in Eq. (33), Eq. (36) involves a sum over every face f of the polyhedron, characterized by its area S_f, outward unit normal vector $\boldsymbol{n}_f$, and specific admittance $\widehat{\beta}_f(k)$.

In the case of the equilateral triangular right prism, Eq. (36) can be deduced from the formulas in McCartin (2004), provided that all the rectangular faces f of this polyhedron (i.e.

the vertical faces in Fig. 1) share the same value $\widehat{\beta}_f(k)$. The wave vectors of the equilateral triangular right prism are represented in 2D in Figs. 5(c) and (d), still in the case of a purely imaginary value of $\widehat{\beta}_f(k)$, using the same conventions as in Figs. 5(a) and (b). Clearly, all comments made in Sec. 7.1 still apply to this case. To sum up, we can make the following observations:

- in the Neumann's case (i.e. if $\widehat{\beta}_f(k) = 0$), the wave vector space is the flat space $\mathbb{R}^3$;
- if $\widehat{\beta}_f(k)$ is purely imaginary (i.e. when there is no energy absorption at the boundary surface), then the wave vector space is still flat and included in $\mathbb{R}^3$, but it undergoes a nonlinear distortion with respect to the Neumann's case (represented in Fig. 5 in the 2D-case);
- if $\widehat{\beta}_f(k)$ is complex but not purely imaginary (i.e. when there is energy absorption), then the wave vector space is the image of the complex function $\boldsymbol{\mathcal{K}}(\boldsymbol{k}, k)$ in Eq. (36), i.e. a curved 3D submanifold of the six-dimensional (over field $\mathbb{R}$) vector space $\mathbb{C}^3$ (represented as the blue curve in Fig. 6 in the 1D-case).

These observations inspire an analogy with the theory of general relativity, which shows that the flat spacetime of special relativity is distorted and curved by the presence of mass. This is actually the reason why in Badeau (2024), we named the version of the statistical wave field theory dedicated to Neumann's boundary condition *special theory* (since the wave vector space is flat in this case), and that dedicated to Robin's boundary condition *general theory* (since the wave vector space is distorted, curved when $\widehat{\beta}_f(k)$ is not purely imaginary, and may contain singularities that behave like black holes when $\mathrm{Im}(\widehat{\beta}_f(k)) > 0$).

7.3. General case (in the wide sense)

Now we would like to find a closed-form expression of the wave vectors distortion that applies to *all* special polyhedra. This is unfortunately not possible by following the simple mathematical approach developed in this paper, for the reasons that were already explained in Sec. 7.2. However, it is possible by generalizing the other, more complex, approach presented in Badeau (2024). For the moment, we keep this generalization for a future publication, but here the correct expression of this wave vectors distortion can already be written and justified with a simple argument. Indeed, as already observed in the case of the rectangular cuboid and the equilateral triangular right prism, the blue lines that represent the repulsors/attractors in Fig. 5 match the ones that characterize the raised spectral measures in Figs. 3(d) and 4(b). So, we can guess that the same property holds in the case of the isosceles right triangular and the hemiequilateral triangular right prisms, whose raised spectral measures were represented in 2D in Figs. 4(a) and (c). Consequently, the general expression of the wave vectors distortion that holds for the four special polyhedra is actually obtained by introducing in Eq. (36) an average over all rotations in C_n, like in Eq. (33):

$$\boldsymbol{\mathcal{K}}(\boldsymbol{k}, k) = \boldsymbol{k} + \tfrac{\imath\lambda}{4\pi} \sum_f S_f \left(\frac{1}{n} \sum_{\boldsymbol{R} \in C_n} \ln \left(\frac{\boldsymbol{n}_f^\top \boldsymbol{R} \boldsymbol{\mathcal{K}}(\boldsymbol{k}, k) + k\, \widehat{\beta}_f(k)}{\boldsymbol{n}_f^\top \boldsymbol{R} \boldsymbol{\mathcal{K}}(\boldsymbol{k}, k) - k\, \widehat{\beta}_f(k)} \right) \boldsymbol{R}^\top \boldsymbol{n}_f \right), \tag{37}$$

which indeed reduces to (36) in the particular cases of the rectangular cuboid and the equilateral triangular right prism. In other respects, it can be noticed from Eq. (37) that $\boldsymbol{\mathcal{K}}(\boldsymbol{R}\,\boldsymbol{k},k) = \boldsymbol{R}\,\boldsymbol{\mathcal{K}}(\boldsymbol{k},k)$ for any rotation $\boldsymbol{R} \in C_n$, which means that rotating the Neumann's wave vectors by any rotation in C_n amounts to rotating the corresponding Robin's wave vectors by the same rotation.

8. Relationship with mixing billiards

Let us now show the relationship between the formulas obtained in this paper and the ones presented in Badeau (2024), which were dedicated to the case of mixing billiards. Contrary to the special polyhedra, where the successive reflections on the faces generate a finite group of rotations C_n, in mixing billiards, the successive reflections on the boundary surface generate an infinite group of rotations that is uniformly dense in SO(3), making the wave field isotropic. In other words, the average over all rotations in C_n that appears in Eqs. (33) and (37) is replaced by an average over all rotations in SO(3). If in addition we replace the sum over the faces f of area S_f by an integral over $\boldsymbol{s} \in \partial V$ with respect to the surface element $dS(\boldsymbol{s})$, then the volume and surface terms in Eq. (33) yield

$$\widehat{M}_B(\boldsymbol{k}) = \lambda + \tfrac{\lambda^2}{4} \int_{\boldsymbol{s}\in\partial V} \left(\tfrac{1}{4\pi} \int_{\boldsymbol{u}\in\mathcal{S}(0,1)} \delta(\boldsymbol{u}^\top \boldsymbol{k}) dS(\boldsymbol{u}) \right) dS(\boldsymbol{s}) = \lambda + \tfrac{\lambda^2 S(\partial V)}{8\|\boldsymbol{k}\|_2}.$$

Since $\widehat{\Gamma}_B(\boldsymbol{k}) = \widehat{M}_B(\boldsymbol{k}) - \lambda^2\delta(\boldsymbol{k})$, for all $k > 0$ we get

$$\widehat{\Gamma}_B(k) \triangleq \int_{\boldsymbol{k}\in\mathcal{S}(0,k)} \widehat{\Gamma}_B(\boldsymbol{k}) dS(\boldsymbol{k}) = 4\pi\lambda \left(k^2 + \tfrac{\lambda S(\partial V)}{8} k \right).$$

This equation is exactly Eq. (80) in Badeau (2024), which is related to the asymptotic expansion of the modal density (Balian and Bloch, 1970), as shown in Badeau (2024, Sec. V). In the same way, if $\widehat{\beta}_f(k)$ is also replaced by the local specific admittance $\widehat{\beta}(\boldsymbol{s},k)$, then Eq. (37) becomes

$$\boldsymbol{\mathcal{K}}(\boldsymbol{k},k) = \boldsymbol{k} + \tfrac{\imath\lambda}{4\pi} \int_{\boldsymbol{s}\in\partial V} \left(\tfrac{1}{4\pi} \int_{\boldsymbol{u}\in\mathcal{S}(0,1)} \ln\left(\tfrac{\boldsymbol{u}^\top \boldsymbol{\mathcal{K}}(\boldsymbol{k},k) + k\,\widehat{\beta}(\boldsymbol{s},k)}{\boldsymbol{u}^\top \boldsymbol{\mathcal{K}}(\boldsymbol{k},k) - k\,\widehat{\beta}(\boldsymbol{s},k)} \right) \boldsymbol{u}\, dS(\boldsymbol{u}) \right) dS(\boldsymbol{s}).$$

This formula can be rewritten in the following form, which explicitly highlights the isotropy of the wave vectors distortion: $\boldsymbol{\mathcal{K}}(\boldsymbol{k},k) = \mathcal{K}(\|\boldsymbol{k}\|_2,k)\frac{\boldsymbol{k}}{\|\boldsymbol{k}\|_2}$, where $\mathcal{K}(K,k) \in \mathbb{C}$ denotes the wave numbers distortion:

$$\mathcal{K}(K,k) = K + \tfrac{\imath\lambda}{8\pi} \int_{\boldsymbol{s}\in\partial V} \left(\ln\left(\tfrac{\mathcal{K}(K,k) + k\widehat{\beta}(\boldsymbol{s},k)}{\mathcal{K}(K,k) - k\widehat{\beta}(\boldsymbol{s},k)} \right) - \left(\tfrac{k\widehat{\beta}(\boldsymbol{s},k)}{\mathcal{K}(K,k)} \right)^2 \ln\left(\tfrac{k\widehat{\beta}(\boldsymbol{s},k) + \mathcal{K}(K,k)}{k\widehat{\beta}(\boldsymbol{s},k) - \mathcal{K}(K,k)} \right) + \tfrac{2k\widehat{\beta}(\boldsymbol{s},k)}{\mathcal{K}(K,k)} \right) dS(\boldsymbol{s}).$$

This last equation is exactly Eq. (102) in Badeau (2024), which contains the seeds of Eyring's formula of the reverberation time (Eyring, 1930), as shown in Badeau (2024, Sec. VI.F).

9. Conclusion

In this paper, we have presented a new version of the statistical wave field theory dedicated to the case of special polyhedra, whose mathematical study proved to be much simpler than that of mixing billiards that was originally addressed in Badeau (2024). In the case of Neumann's boundary condition, we were able to determine directly the first and second order statistics of the B-function by exploiting its periodicity over space. The case of Robin's boundary condition was even simpler: we were able to determine the anisotropic distortion of the wave vectors directly from their closed-form expression. In both cases, the theory predictions hold at all frequencies, which is another difference with respect to the mixing case, which only holds at high frequency.

Though limited to only a few polyhedra, the new approach developed here offered a very interesting insight into the theory, and permitted us to introduce several new concepts: the *edge* and *vertex* terms that appear in the expression of the spectral measure in Neumann's case, and the *repulsors*, *attractors* and *black holes* that appear in the distorted wave vectors space in Robin's case. In addition, it gave us a first glimpse on the general formulas that hold in the broader context of anisotropic wave fields.

Although this new mathematical approach is very different from the one that we originally developed in Badeau (2024), the formulas that we obtained are closely related to those presented in Badeau (2024), as shown in Sec. 8. This gives us a high confidence in the validity of the results presented in both papers, since two different mathematical paths involving various concepts from different areas of mathematics (Weyl-like asymptotic laws and dynamical billiards on the first hand, geometry and crystallography on the other hand) converged to the same conclusions.

In future work, we will present a unified version of the theory dedicated to anisotropic wave fields, which encompasses both cases of special polyhedra and mixing billiards. This will be achieved by generalizing the approached developed in Badeau (2024) to the case of non-ergodic billiards in which space is still explored uniformly over time. In addition, we will also provide general expressions of the edge and vertex terms that have been introduced here, in order to complement the second order curvature term that we already investigated in Badeau (2025). The improved predictions of the theory will then hold at lower frequencies for a large variety of geometric shapes, including both curved surfaces and edges/vertices.

Acknowledgments

The author would like to thank the anonymous reviewers for their very helpful comments.

Author Declarations

Conflict of Interest: The author of this paper has no conflict of interest to disclose.

Data Availability

Data sharing is not applicable to this article as no new data were created or analyzed in this study.

References

Amar, V., Pauri, M., and Scotti, A. (**1991**). "Schrödinger equation for convex plane polygons: A tiling method for the derivation of eigenvalues and eigenfunctions," J. Math. Phys. **32**(9), 2442–2449.

Arnold, V. I., and Avez, A. (**1989**). *Ergodic problems of classical mechanics* (Addison-Wesley, Boston).

Badeau, R. (**2024**). "Statistical wave field theory," J. Acoust. Soc. Am. **156**(1), 573–599.

Badeau, R. (**2025**). "Statistical wave field theory: Curvature term," J. Acoust. Soc. Am. **157**(3), 1650–1664.

Balian, R., and Bloch, C. (**1970**). "Distribution of eigenfrequencies for the wave equation in a finite domain: I. Three-dimensional problem with smooth boundary surface," Ann. Phys. **60**(2), 401–447.

Bamberg, J., Cairns, G., and Kilminster, D. (**2003**). "The crystallographic restriction, permutations, and Goldbach's conjecture," The American Mathematical Monthly **110**(3), 202–209.

Blom, M. (**2021**). "Classifying strictly tessellating polytopes," Master's thesis, Chalmers University of Technology, Gothenburg, Sweden.

Bravais, A. (**1850**). "Mémoire sur les systèmes formés par les points distribués régulièrement sur un plan ou dans l'espace (*Dissertation on the systems formed by points regularly distributed on a plane or in space*)," Journal de l'École Polytechnique **19**, 1–128.

Burzlaff, H., and Zimmermann, H. (**2006**). "Point-group symbols," in *International Tables for Crystallography, Online MRW*, **vol. A** (John Wiley & Sons, Ltd, Hoboken, New Jersey), Chap. 12.1, pp. 818–820.

Cook, R. K., Waterhouse, R., Berendt, R., Edelman, S., and Thompson, M. (**1955**). "Measurement of correlation coefficients in reverberant sound fields," J. Acoust. Soc. Am. **27**(6), 1072–1077.

Daley, D. J., and Vere-Jones, D. (**2003**). Probability and its Applications *An introduction to the theory of point processes. Volume I: Elementary Theory and Methods*, 2nd ed. (Springer-Verlag, New York).

Eyring, C. F. (**1930**). "Reverberation time in 'dead' rooms," J. Acoust. Soc. Am. **1**(2A), 217–241.

Joyce, W. B. (**1975**). "Sabine's reverberation time and ergodic auditoriums," J. Acoust. Soc. Am. **58**(3), 643–655.

Joyce, W. B. (**1978**). "Exact effect of surface roughness on the reverberation time of a uniformly absorbing spherical enclosure," J. Acoust. Soc. Am. **64**(5), 1429–1436.

Kuttruff, H. (**2014**). *Room Acoustics, 5th ed.* (CRC Press, Boca Raton, FL), pp. 1–374.

Lamé, G. (**1833**). "Mémoire sur la propagation de la chaleur dans les polyèdres (*Dissertation on heat propagation in polyhedra*)," Journal de l'École Polytechnique **22**, 194–251.

McCartin, B. J. (**2002**). "Eigenstructure of the equilateral triangle, Part II: The Neumann problem," Mathematical Problems in Engineering **8**(6), 517–539.

McCartin, B. J. (**2004**). "Eigenstructure of the equilateral triangle. Part III: The Robin problem," International Journal of Mathematics and Mathematical Sciences **2004**(16), 807–825.

McCartin, B. J. (**2008**). "On polygonal domains with trigonometric eigenfunctions of the Laplacian under Dirichlet or Neumann boundary conditions," Applied Mathematical Sciences **2**(58), 2891–2901.

McCartin, B. J. (**2011**). *Laplacian eigenstructure of the equilateral triangle* (Hikari Ltd., Ruse, Bulgaria).

Moorer, J. A. (**1979**). "About this reverberation business," Computer Music Journal **3**(2), 13–28.

Morse, P. M., and Ingard, K. U. (**1968**). *Theoretical acoustics* (McGraw-Hill, New York).

Overfelt, P., and White, D. (**1986**). "TE and TM modes of some triangular cross-section waveguides using superposition of plane waves (short paper)," IEEE Transactions on Microwave Theory and Techniques **34**(1), 161–167.

Pearson, D. B. (**2001**). "Sturm–Liouville theory," in *Encyclopedia of Mathematics* (EMS Press, Berlin).

Pelat, A., Gautier, F., Conlon, S. C., and Semperlotti, F. (**2020**). "The acoustic black hole: A review of theory and applications," Journal of Sound and Vibration **476**(115316).

Polack, J.-D. (**1988**). "La transmission de l'énergie sonore dans les salles (*The transmission of sound energy in rooms*)," Ph.D. thesis, Université du Maine, Le Mans, France.

Polack, J.-D. (**1992**). "Modifying chambers to play billiards: the foundations of reverberation theory," Acta Acust. united Acust. **76**(6), 256–272(17).

Polack, J.-D. (**2024**). "Revisiting reverberation formulae," INTER-NOISE and NOISE-CON Congress and Conference Proceedings **270**, 3497–3504.

Rowlett, J., Blom, M., Nordell, H., Thim, O., and Vahnberg, J. (**2021**). "Crystallographic groups, strictly tessellating polytopes, and analytic eigenfunctions," The American Mathematical Monthly **128**(5), 387–406.

Schroeder, M. R. (**1962**). "Frequency-correlation functions of frequency responses in rooms," J. Acoust. Soc. Am. **34**(12), 1819–1823.

Tabachnikov, S. (**1995**). Panoramas et synthèses *Billiards* (Société mathématique de France, Paris, France).